

## Full length article

## Achieving ultra-high strength and ductility in equiatomic CrCoNi with partially recrystallized microstructures

C.E. Slone <sup>a, b</sup>, J. Miao <sup>a, b</sup>, E.P. George <sup>c, d</sup>, M.J. Mills <sup>a, b, \*</sup><sup>a</sup> Center for Electron Microscopy and Analysis, The Ohio State University, Columbus, OH, 43212, USA<sup>b</sup> Department of Materials Science and Engineering, The Ohio State University, Columbus, OH, 43210, USA<sup>c</sup> Materials Science and Technology Division, Oak Ridge National Laboratory, Oak Ridge, TN, 37831, USA<sup>d</sup> Materials Science and Engineering Department, University of Tennessee, Knoxville, TN, 37996, USA

## ARTICLE INFO

## Article history:

Received 11 September 2018

Received in revised form

7 December 2018

Accepted 9 December 2018

Available online 11 December 2018

## Keywords:

High and medium entropy alloys

Ultra-high strength

Twinning

High ductility

Heterogeneous microstructure

## ABSTRACT

Despite having otherwise outstanding mechanical properties, many single-phase medium and high entropy alloys are limited by modest yield strengths. Although grain refinement offers one opportunity for additional strengthening, it requires significant and undesirable compromises to ductility. This work therefore explores an alternative, simple processing route to achieve strength by cold-rolling and annealing an equiatomic CrCoNi alloy to produce heterogeneous, partially recrystallized microstructures. Tensile tests reveal that our approach dramatically increases the yield strength (to ~1100 MPa) while retaining good ductility (total elongation ~23%) in the single-phase CrCoNi alloy. Scanning and transmission electron microscopy indicate that the strengthening is due to the non-recrystallized grains retaining their deformation-induced twins and very high dislocation densities. Load-unload-reload tests and grain-scale digital image correlation are also used to study the accumulation of plastic deformation in our highly heterogeneous microstructures.

© 2018 Acta Materialia Inc. Published by Elsevier Ltd. All rights reserved.

## 1. Introduction

Certain multi-principal element (MPE) alloys such as equiatomic, single phase CrCoNi [1–3] and CrCoFeMnNi [4–6] are now well-known for their outstanding combinations of high hardening rates, large ductility, and excellent fracture toughness at ambient and cryogenic temperatures. Despite their recent development [7,8], these alloys already exhibit superior properties relative to more conventional alloys, including many twinning induced plasticity (TWIP) and transformation induced plasticity (TRIP) steels [9,10]. The desirable mechanical properties noted above arise from a complex set of deformation mechanisms at the nanoscale; however, one major limitation for these MPE alloys is a modest yield strength, which benefits only from a solid solution effect and not the extremely refined microstructures that develop in association with large deformations [3]. One key challenge for these alloys (and all structural materials) is therefore the development of a method for increasing the yield strength while retaining substantial

ductility. This work explores one possible route for achieving that objective with a simple processing method that leads to tunable combinations of ultra-high strength and ductility.

The tensile response and deformation mechanisms of single-phase face-centered cubic (fcc) equiatomic alloys CrCoFeMnNi [6,11–14], CrCoFeNi [15,16], and CrCoNi [3,5,15,17–19] have all been thoroughly studied in the fully recrystallized state. These alloys have relatively low stacking fault energies [20–22] that promote dissociation of perfect dislocations into  $a/6\langle 112 \rangle$  partial dislocations at low strains; further deformation results in the development of nanotwins that serve as potent barriers to dislocation motion, generating the macroscopically observed high hardening rates. The hardening is further enhanced in CrCoNi [3] and CrCoFeNi [16] by a highly localized interfacial phase transformation that produces hexagonal close-packed (hcp) regions along stacking faults and, most prominently, deformation twins. The transformation has also been observed in CrCoFeMnNi under high pressure [23,24], but not after tensile deformation or rolling. Although the volume fraction of this transformation product is very low, in contrast to other materials benefitting from the TRIP effect, slip transmission from the fcc matrix across hcp-lined nano-twins is prohibitively difficult [21]. This has recently been shown to enhance the hardening

\* Corresponding author. Center for Electron Microscopy and Analysis, The Ohio State University, 1305 Kinnear Rd, Columbus, OH 43212, USA.

E-mail address: [mills.108@osu.edu](mailto:mills.108@osu.edu) (M.J. Mills).

behavior beyond that in conventional TWIP materials [25].

Despite the confluence of desirable properties described above, one limiting factor in the application of these materials is their modest yield strength. For CrCoNi with grain sizes of 15–25  $\mu\text{m}$ , the room-temperature yield strength is  $\sim 375$  MPa [2,25]. The other fcc single-phase alloys described above have even lower yield strengths [15]. Recently, progress has been made in enhancing the yield strength of TWIP steels by rolling and annealing the material at modest temperatures to induce recovery while preserving the deformation twins [26–30]. It is proposed that the remaining twin structures enhance the yield strength of the material on subsequent deformation while some ductility is restored by reducing the total dislocation density. This processing strategy also tends to produce partially recrystallized microstructures with spatial gradients in grain size as well as stored deformation content. A similar rolling and annealing process was recently employed in MPE alloys to achieve good combinations of strength and ductility. For example, a partially recrystallized VCrMnFeCoNi alloy was first shown to exhibit a room-temperature yield strength of  $\sim 760$  MPa and  $\sim 28\%$  elongation to failure [31] whereas a partially recrystallized CrCoFeMnNi alloy was shown to exhibit a yield strength of  $\sim 600$  MPa and  $\sim 27\%$  ductility [32]. The same rolling and annealing strategy was also recently utilized to produce ultra-high yield strength of 1100 MPa and 30% ductility in a Ni–Cr–Co superalloy containing precipitates, although deformation twinning was not observed in that material [33].

Heavy deformation followed by annealing has also been studied in equiatomic CrCoNi [34] and has very recently been shown to produce dramatic improvements in the shear strength [35] and in strength/ductility combinations during tensile deformation [36] although questions remain about the underlying mechanisms. Schuh et al. [34] used high-pressure torsion that, while useful for probing fundamental behavior, often produces highly non-equilibrium microstructures that are not attainable using conventional processes like rolling. In the latter two studies [34,35], some key results for the heterogeneous microstructures have not been compared to results from the homogeneous, fully recrystallized material. For example, the outstanding strength and ductility reported for partially recrystallized CrCoNi in Ref. [36] was purported to originate from large back-stresses developed in nanoscale recrystallized grains based on the large hysteresis observed in load-unload-reload tests. New results from the present study suggest that explanation may be incomplete since it will be shown that similar hysteresis is also observed in homogeneous fully recrystallized material with larger, more conventional grain sizes. Additionally, although there are some preliminary indications that heterogeneous microstructures obtained by partial recrystallization may be beneficial for single-phase, concentrated solid solution alloys, there are still many open questions regarding 1) the extent of the strengthening effect, and the tradeoff with ductility; 2) the relationship between processing parameters and the tensile properties; and 3) the mechanism by which improvements in strength and ductility occur, when such an effect is observed. Note that for any real improvement, the effect must be above and beyond what could be achieved with grain refinement alone.

In this work, we examine the influence of a heterogeneous microstructure on equiatomic CrCoNi alloy produced by cold-rolling and annealing. The combination of a multi-modal grain size distribution with residual deformation structures is shown to produce a three-fold increase in yield strength to values exceeding 1 GPa while retaining good uniform elongation. In contrast to previous studies, heterogeneous and homogeneous microstructures are thoroughly compared and the grain-scale distribution of plastic strain is measured.

## 2. Experiments

### 2.1. Material

Ingots of equiatomic CrCoNi were produced by arc melting pure ( $>99.9\%$ ) constituent metals under Ar atmosphere followed by drop-casting into a copper mold. Prior to drop-casting, the buttons were flipped and re-melted to ensure mixing. The cast ingots were homogenized in vacuum for 24 h at 1200 °C (1473 K) before cold-rolling to a reduction in thickness of approximately 70%. The above processing steps are similar to those employed in previous publications [3,8].

Rolled plates were cut by wire electrical discharge machining (EDM) into cubes for hardness measurements or flat tensile specimens with nominal gauge dimensions 5 mm (length)  $\times$  2 mm (width)  $\times$  1.2 mm (thickness) and grip widths of 3 mm. The longitudinal (tensile) axes of the specimens were aligned with the rolling direction of the original plate and the faces were parallel to the plate. After fabrication by EDM, hardness and tensile specimens were annealed in air at temperatures between 600 °C (873 K) and 900 °C (1173 K) and times between 15 min and 12 h. The furnace was pre-heated before sample insertion and heat treatments were considered to start when the specimen temperature was within 3 °C of the target temperature, which typically took between 4 and 7 min. Specimens were air-cooled following annealing. Some additional specimens were heated using slow temperature ramps of 10 °C/minute up to 300 °C followed by 3 °C/minute up to the target temperature (e.g. 600 °C).

### 2.2. Hardness measurement and mechanical testing

Following heat treatment, specimens for hardness testing were mechanically polished using 400-, 600-, 800-, and 1200-grit SiC paper. Hardness measurements were made on a Leco LM-100AT microhardness tester with a loading force of 100 g and dwell time of 25 s. For each specimen, an array of  $6 \times 6$  indents was made on both ends of the specimen for a total of 72 measurements per condition. The spacing between indents was 100  $\mu\text{m}$  and the typical size of each indent on the surface was on the order of 20  $\mu\text{m}$ .

Tensile specimens were polished on the faces and sides of the gauge section using 400-, 600-, and 800-grit SiC paper. Uniaxial tensile testing was performed on an Instron Electrothermal Mechanical Tester (ETMT) with engineering strain rates of  $5\text{--}10 \cdot 10^{-4} \text{ s}^{-1}$ . Strain measurements were made using digital image correlation (DIC) with paint patterns applied to the surface of the specimens. Full-field strain maps were produced with Correlated Solutions VIC2D software [37] using subset and step sizes of approximately 0.65 mm and 0.01 mm, respectively. Engineering strain was determined through conversion of the average Lagrangian strain in the gauge section as calculated by VIC2D. True stress and strain were calculated from engineering values assuming a constant volume during plastic deformation. Load-unload-reload (LUR) tensile tests were performed with the same conditions described above and each unloading occurring over a fixed time of 10 s.

### 2.3. Scanning and transmission electron microscopy

Pre- and post-deformation specimens were prepared for study in the SEM using a parallel polisher and 400-, 600-, 800-, and 1200-grit SiC papers. A final chemo-mechanical polish was performed using 50 nm colloidal silica. The nominally equiatomic alloy composition was confirmed using semi-quantitative X-ray energy dispersive spectroscopy (EDS).

Specimens were examined using a ThermoFisher/FEI Apreo

scanning electron microscope (SEM). Electron backscatter diffraction (EBSD) orientation mapping was performed using an EDAX Hikari Super EBSD camera in conjunction with acquisition software EDAX TSL DC7 and analysis software EDAX TSL OIM 8 [38]. Scans were acquired using an accelerating voltage of 20 kV and a beam current of 6.4 nA at a working distance of 20 mm; scans shown in this work and used for calculating recrystallized area fractions and grain sizes were  $62 \times 62 \mu\text{m}$  with a step size of 100 nm.

Lift-out TEM specimens were prepared using a FEI Helios Nanolab 600 dual beam system. All TEM foils were further cleaned before observation in a Fischione Model 1040 nanomill system at low voltages. Low magnification STEM images and selected area diffraction patterns were obtained using a FEI Tecnai F20 S/TEM microscope operating at 200 kV. STEM-EDS maps were collected using a Super-X Energy Dispersive Spectrometry (Super-X EDS) system in a FEI Titan G2 60-300 microscope at 300 kV. Atomic resolution HAADF-STEM imaging was conducted in a probe-corrected FEI Titan 80–300 S/TEM microscope at an accelerating voltage of 300 kV. Scanning distortion and noise in STEM images were further reduced via nonlinear drift distortion correction [39].

#### 2.4. Local strain measurement by digital image correlation

*Ex situ* scanning electron microscopy digital image correlation (SEM-DIC) was used to study strain localization in partially recrystallized microstructures. Regions of interest for strain mapping were identified using a backscattered electron detector and marked via *in situ* platinum deposition. Orientation maps of these regions were generated using EBSD for later alignment with strain maps. Following this initial characterization, patterns were applied to the surface of the specimens with nominally 50 nm colloidal alumina and acquired using the in-column T1 detector. A reference pattern was also created on a separate specimen to measure the distortions introduced by the *ex situ* measurement technique; since the reference pattern would not experience any deformation, any strain measured via DIC on that specimen was considered as error. Following acquisition of images for the region of interest and the reference pattern, specimens were removed from the SEM, tensile tested on the ETMT with the same parameters described in the previous section, and returned to the SEM for post-deformation imaging.

The T1 detector, which produces signal from a combination of secondary and backscattered electrons, was found to provide good contrast between the pattern and the material while minimizing unwanted background contrast from grain orientation or surface topography. SEM images with dimensions of  $3072 \times 2048$  pixels were acquired using a 10  $\mu\text{s}$  dwell time with a horizontal field width of 207  $\mu\text{m}$  (corresponding to a magnification of 1000 $\times$  in the Thermofisher/FEI Apreo SEM used for this study). This produced an image resolution of approximately 67 nm/pixel. Since sub-micron realignment of the specimen in the SEM was not possible between each tensile experiment, images were later aligned manually at their centers before implementation of the DIC algorithm in Correlated Solutions' VIC-2D 2009 software [37]. Subset and step sizes for image correlation were 33 pixels ( $\sim 2200$  nm) and 5 pixels ( $\sim 340$  nm), respectively.

### 3. Results

#### 3.1. Microstructure following rolling and annealing

Following room temperature rolling to 70% reduction in thickness and subsequent annealing at different temperatures and times, the equiatomic CrCoNi alloy exhibited microstructures with varying degrees of recrystallization. In our analysis, recrystallized

grains were defined as those with less than  $1^\circ$  of intragranular misorientation. Fig. 1 shows EBSD grain orientation maps for three different annealing conditions. The top row of images shows the full microstructure and contains all points measured with confidence index greater than 0.1. In contrast, the bottom row of images shows the same regions but only contains points belonging to recrystallized grains. This separation highlights the substantial increase in the fraction of recrystallized grains over a relatively small range of conditions. Segmentation of EBSD results showed approximately  $39 \pm 3\%$  (standard error) of the volume was recrystallized following annealing at  $600^\circ\text{C}/1$  h;  $76 \pm 2\%$  of the volume was recrystallized following annealing at  $600^\circ\text{C}/4$  h; and a fully recrystallized microstructure was produced following annealing at  $700^\circ\text{C}/1$  h. Fig. S1 in the supplementary information also shows microstructures corresponding to the rolling, transverse, and normal directions for the  $600^\circ\text{C}/1$  h condition.

The microstructure after cold-rolling and annealing at  $600^\circ\text{C}/1$  h was further examined via scanning transmission electron microscopy (STEM), as shown in Fig. 2. One important question regarding this alloy was whether deformation twins produced during rolling could be preserved at temperatures high enough to promote dislocation annihilation and recovery. If so, a partially-recovered microstructure could confer higher strength due to the retained twins while restoring some ductility via recovery and lower dislocation density. The low-magnification  $\langle 101 \rangle$  zone axis STEM image in Fig. 2a and the corresponding diffraction pattern in Fig. 2b unambiguously confirm the presence of deformation twins (fine, dark linear features) on  $\{111\}$ -type planes after annealing at  $600^\circ\text{C}/1$  h. The diffraction pattern also shows elevated intensity at peaks corresponding to the hcp phase. Both deformation twinning and hcp structure are explicitly observed via high-resolution HAADF-STEM, Fig. 2c and d. As previously shown for this alloy, hcp formation is limited to a few atomic layers and occurs at the interfaces along deformation twins [25,40]. These results clearly demonstrate that twin/hcp structures produced during rolling are preserved even after annealing at elevated temperatures.

Energy dispersive x-ray spectroscopy (EDS) chemical mapping did not show any evidence for elemental segregation or phase decomposition at coarser SEM length scales ( $10^1$ – $10^3 \mu\text{m}$ ) or finer TEM length scales ( $10^1$ – $10^3$  nm). Fig. 3 shows results at finer length scales from two regions in the rolled and annealed  $600^\circ\text{C}/1$  h condition. The first region in Fig. 3a shows both large dislocation tangles and a network of deformation twins (bright linear features noted by arrows). Fig. 3b shows a higher magnification image of a single deformation twin. In both cases, the average composition over the scanned region (Table 1) was in good agreement with bulk composition measurements. Although no apparent elemental segregation was observed at either magnification, the large dislocation density and associated strain may obscure compositional heterogeneities, particularly at very fine length scales. Further study of this effect is in progress.

Grain size distributions were estimated based on EBSD data. As previously noted, the step size used for EBSD measurements was 100 nm and regions were only classified as grains for measurement purposes if they contained multiple rows and had diameters greater than or equal to 500 nm (i.e. sampled by at least five points). An area-weighted average was used to determine the representative grain size since weighting by area rather than number is more robust against the number of points used in sampling each grain as well as the effect of multi-modal grain size distributions [41–43]. The data were separated for recrystallized and non-recrystallized grains and are shown in Fig. 4 for selected conditions. For the recrystallized grains following annealing at  $600^\circ\text{C}/1$  h, the area-weighted average grain diameter was approximately  $1.6 \pm 0.0 \mu\text{m}$  (standard error) and had a distribution shifted towards smaller

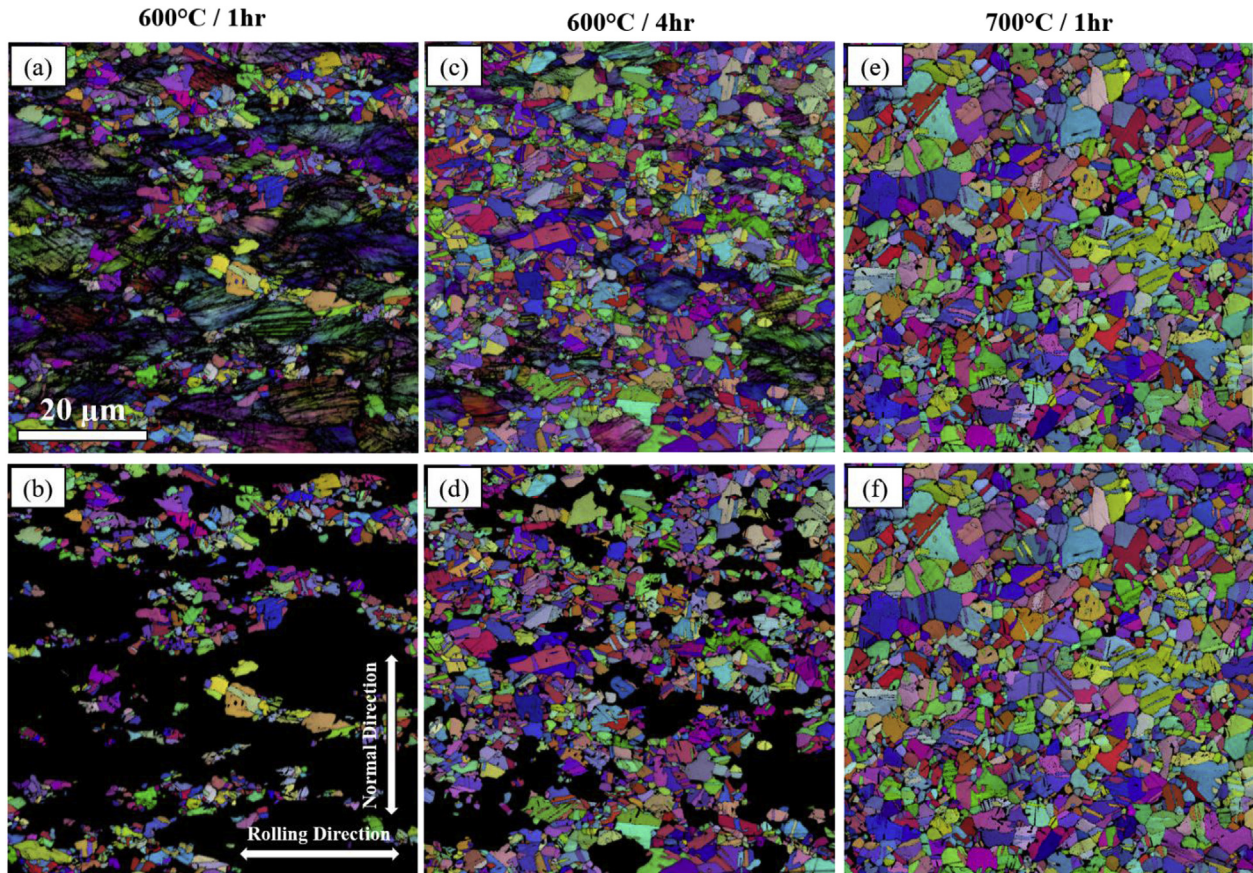


**Fig. 1.** EBSD from CrCoNi after rolling (70% thickness reduction) and annealing at (a) and (b), 600 °C/1hr; (c) and (d), 600 °C/4hr; and (e) and (f), 700 °C/1hr. The images in the top row include all grains; the bottom row of images shows only recrystallized grains with intragranular misorientation  $<1^\circ$ .

grains compared to the distributions of the 600 °C/4 h and the 700 °C/1 h (fully recrystallized) conditions with average diameters of  $2.0 \pm 0.1$  and  $2.3 \mu\text{m}$ , respectively. This suggests very modest grain growth occurred for the latter two conditions. It is also interesting to note that the 600 °C/4 h and 700 °C/1 h conditions had very similar size distributions for the recrystallized grains despite having different volume fractions (about 76% in the 600 °C/4 h condition compared to full recrystallization in the 700 °C/1 h specimen). This feature was especially useful in comparing the mechanical response of the different conditions, as will be discussed later. Annealing at 900 °C/1 h also produced a fully recrystallized microstructure that experienced significant grain growth resulting in an average grain size of approximately  $24 \mu\text{m}$ .

### 3.2. Hardness and tensile response following rolling and annealing

After 70% reduction in thickness by room-temperature rolling, the average hardness of the CrCoNi alloy was 468 HV with minimum and maximum values of 445 HV and 495 HV. Conventional recovery and recrystallization behavior were observed after exposure to temperatures above 600 °C. Fig. 5a and b shows the change in hardness as a function of annealing temperature and time, respectively. Higher annealing temperatures expedited recovery and recrystallization kinetics and produced a more pronounced softening effect relative to the as-rolled material, which is also shown for reference in Fig. 5. Following annealing at 900 °C/1 h, which is a common heat treatment applied to this alloy to produce a fully recrystallized microstructure after rolling, the hardness decreased to 222 HV. Longer annealing treatments at 600 °C also

produced substantial softening although even after 12 h the average hardness remained at 352 HV. As shown in Fig. 5b, the small change between the 4 h and 12 h heat treatments at 600 °C suggests the remaining deformation structures were relatively stable at this temperature.

The bars associated with each data point in Fig. 5a and b shows the minimum and maximum hardness measured at each condition. Annealing at temperatures below 700 °C produced substantial scatter in the hardness values as manifested by the large spread around data points corresponding to 600 °C, 625 °C, and 650 °C in Fig. 5a. Examination of the corresponding grain structures in Fig. 1 indicates that partial recrystallization occurred at temperatures below 700 °C, while annealing at that temperature and above produced fully recrystallized microstructures. Scatter in the data is therefore associated with sampling regions in various states of recovery or recrystallization. Individual indents ( $\sim 20 \mu\text{m}$ ) would also be expected to sample many grains for heat treatments in the range of 600–700 °C (grain sizes  $\sim 2 \mu\text{m}$ ) but only 1–3 grains for the 900 °C heat treatment (grain sizes  $\sim 24 \mu\text{m}$ ).

The hardness measurements corresponding to the 600 °C/30min condition show a surprising increase relative to the as-rolled condition (Fig. 5b). This anomalous hardening behavior also manifests in the 600 °C/1 h condition where the maximum value exceeds the maximum observation in the as-rolled material and the average hardness is similar to the as-rolled condition despite some recrystallization having occurred. These specimens were carefully examined in both the scanning electron microscope and transmission electron microscope and no precipitation or other annealing-induced phase transformations were observed. Similar

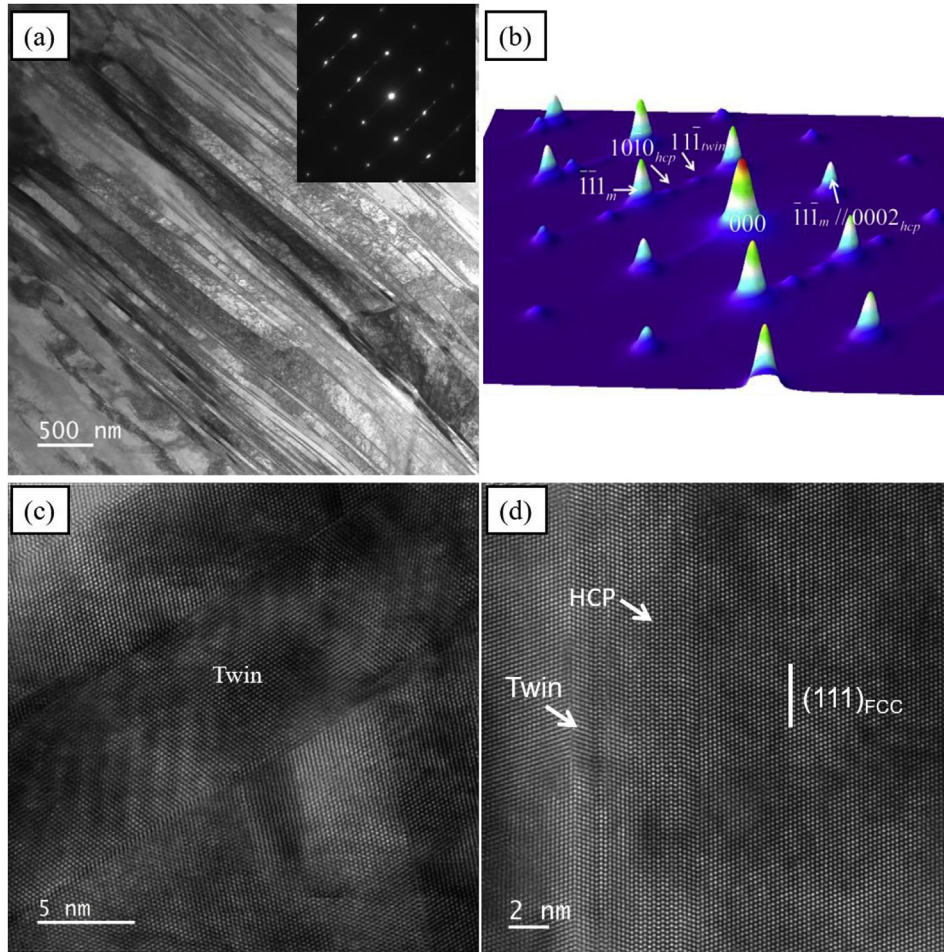


**Fig. 2.** Residual deformation structures following rolling and annealing at 600 °C/1 h: (a) low magnification BF-STEM image (zone axis close to  $\langle 101 \rangle$ ) with inset selected area diffraction pattern; (b) 3D plot of the diffraction pattern from Fig. 2a confirming the presence of both deformation twins and the hcp phase; (c) and (d) high resolution HAADF-STEM images showing deformation twins and the hcp phase.

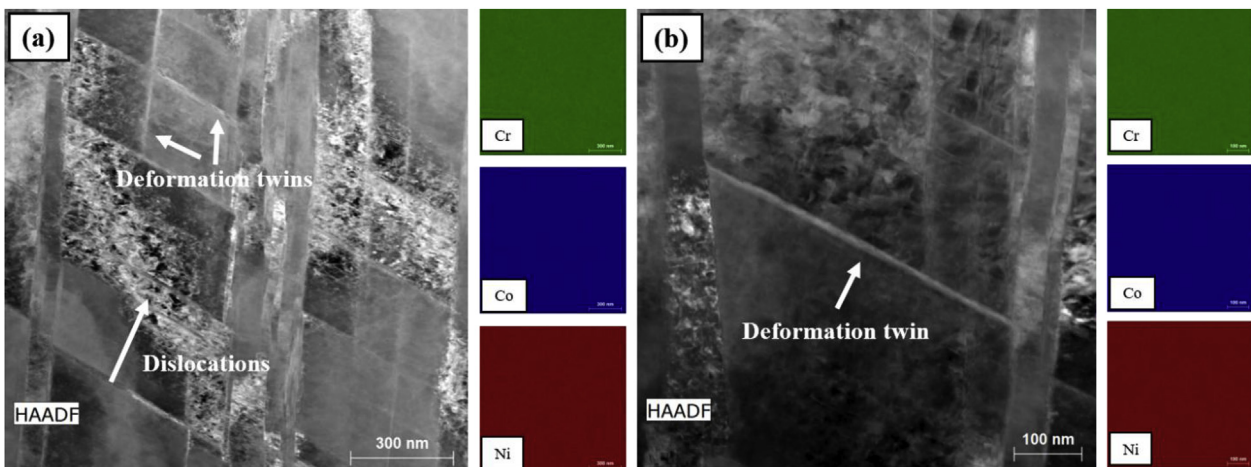


**Fig. 3.** STEM-EDS mapping indicates a homogeneous distribution of elements following rolling and annealing at 600 °C/1 h. Chemical maps were acquired from the same region as shown in the corresponding HAADF images. (a) Coarser length scale showing multiple deformation twins and regions of high dislocation density; (b) finer length scale showing an individual deformation twin.

observations have previously been made in hardness measurements following severe deformation and annealing in CrCoMnFeNi [44–46] and very recently in CrCoNi [34]. This effect is currently

being investigated in greater detail to understand the origin of the observed hardness increase.

The tensile response of the alloy for several selected conditions

**Table 1**  
Standard-less EDS results for the average composition in Fig. 3a and b.

	Element	Atomic Number	[norm. wt.%]	[norm. at.%]	Error in wt.% (1 Sigma)
Fig. 3a	Chromium	24	29.5	32.2	0.9
	Cobalt	27	34.7	33.4	1.1
	Nickel	28	35.7	34.5	1.1
Fig. 3b	Chromium	24	29.5	32.1	0.9
	Cobalt	27	34.7	33.4	1.1
	Nickel	28	35.8	34.5	1.1

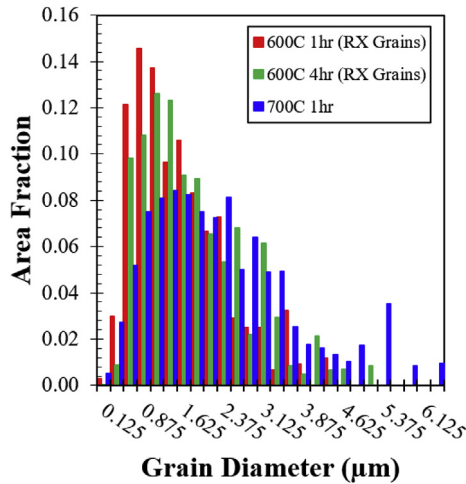


**Fig. 4.** Grain size distributions for (a) recrystallized grains, including the fully recrystallized microstructure after annealing at 700°C/1 h; and (b), non-recrystallized grains.

is indicated in Fig. 6. Additional conditions and the full set of curves for each individual condition (between three and five tests) are included in Fig. S2 of the supplementary information. The yield strength was highest in the as-rolled condition and decreased with longer annealing times and especially higher annealing temperatures. The engineering stress-strain response after annealing at 900°C/1 h represents that for the fully recrystallized alloy with a grain size of 24 µm, and is similar to results published by Laplanche et al. [2] and Miao et al. [3]. As noted previously in this work,

annealing at a lower temperature of 700°C/1 h also produced a fully recrystallized microstructure but with an order of magnitude smaller grain size (2.2 µm compared to 24 µm). Comparison of the 900°C/1 h and 700°C/1 h conditions illustrates the severity of the strength/ductility tradeoff introduced by a reduction in grain size; for this alloy, that reduction increased the yield strength from approximately  $346 \pm 2$  MPa to  $597 \pm 1$  MPa at the cost of a decrease in ductility from 44% uniform elongation to 28% uniform elongation. These results, and new estimates based on figures from the Hall-Petch study by Yoshida et al. [18], suggest that a fully recrystallized microstructure with ultra-high yield strength of 1 GPa would have low uniform elongation of only around 2–5% (see Fig. S3 in the supplementary information).

In contrast, the partially recrystallized microstructures corresponding to conditions of 600°C/1 h and 600°C/4 h produced outstanding tensile properties. The average yield strengths of those conditions were  $1112 \pm 9$  MPa and  $797 \pm 8$  MPa with uniform elongations of 6% and 19% (total elongations of 23% and 34%), respectively. The hardening behavior ( $d\sigma/d\epsilon$ ) for each condition is shown in Fig. 6b with the curves marked to indicate the end of uniform elongation, which was defined by the well-known Considère criterion [47]. Excepting the as-rolled material, the other conditions exhibited similarly shaped hardening curves with two distinct regions typical for this alloy. At low strains, the hardening rate decreased rapidly (region I) followed by a change in slope (region II) that has previously been linked to the occurrence of deformation twinning in fully recrystallized high entropy alloys [6] and TWIP steels [48]. These curves are explicitly compared to the effect of grain size reduction in the supplementary information (Fig. S3c).

It has very recently been argued that heterogeneous grain

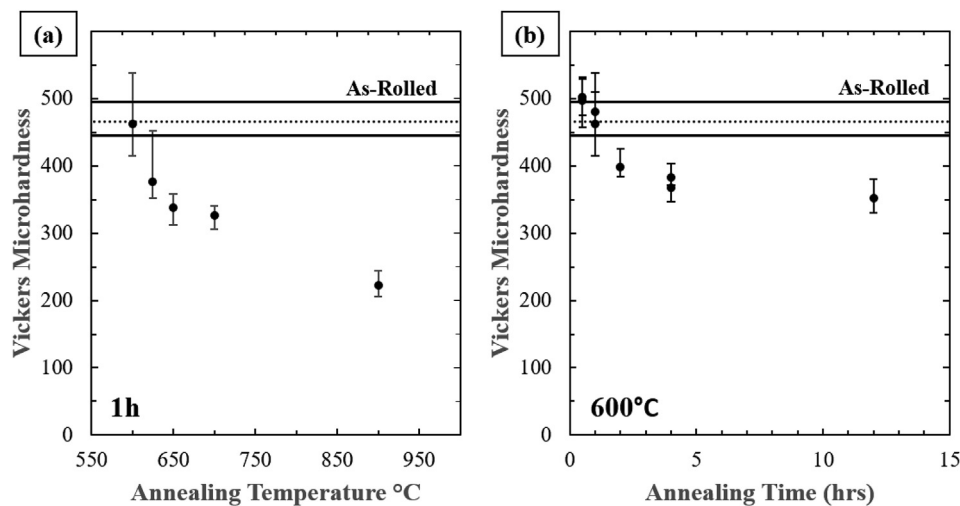


**Fig. 5.** Vickers hardness as a function of (a) annealing temperature for a constant annealing time of 1 h; and (b) annealing time for a constant temperature of 600°C. Data points indicate average values and bars indicate the minimum and maximum hardness values to convey the spread in the data. Multiple data points for the same time indicate independent annealing and measurement of multiple specimens.

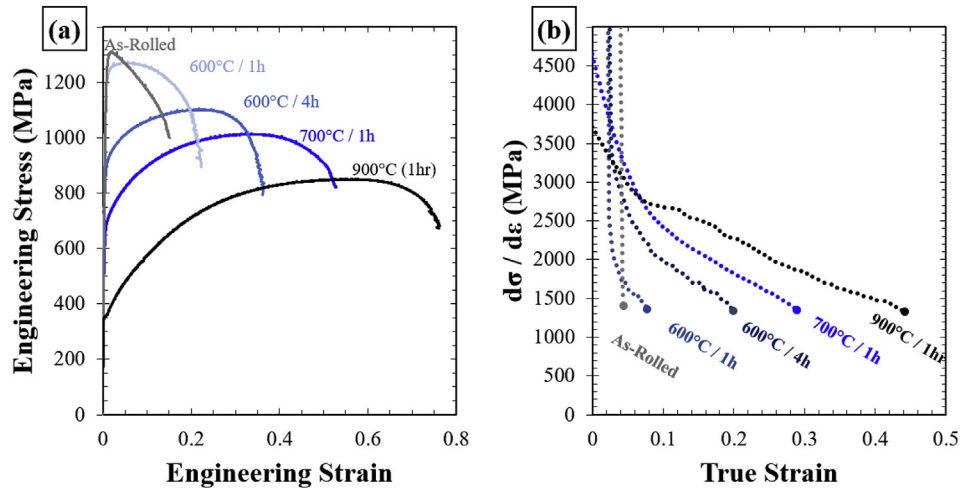


**Fig. 6.** Results of mechanical tests on CrCoNi in the as-rolled state and after varying degrees of partial and full recrystallization. Curves in (a) show the tensile response corresponding to different heat treatments; (b) shows the strain hardening response for each condition. The end of uniform elongation (where  $d\sigma_{\text{true}}/d\varepsilon = \sigma_{\text{true}}$ ) is marked on each curve.

structures enhance the mechanical properties of CrCoNi through a back-stress effect that can be clearly observed during load-unload-reload (LUR) tensile testing [36]. LUR testing was also performed in this study to compare behavior in the partially recrystallized (heterogeneous) condition to the fully recrystallized (uniform grain size) condition and the results for both are shown in Fig. 7. As previously reported, a large hysteresis effect indicative of substantial back-stresses was observed in the partially recrystallized material (blue curve in Fig. 7a). In comparison, the hysteresis loops for the fully recrystallized material strained to the same levels were much smaller (red curve in Fig. 7a). It is worth noting that, for the strains in Fig. 7a, the stresses in the fully recrystallized material are much lower than those in the partially recrystallized material because of its lower flow strength, which is obvious from examination of the curves but has not been remarked upon in other recent work. With increasing stress, the width of the loops increased, even for the fully recrystallized state. When the two microstructural conditions were compared at the same level of true stress, as shown in Fig. 7b, the hysteresis effect was essentially

identical. Note that the level of true stress shown in Fig. 7b (approximately 1040 MPa) is reached almost immediately in the partially recrystallized material at a true strain of about 1%; in contrast, it was only attainable in the fully recrystallized material after substantial work hardening and corresponded to a true strain of approximately 26%. The similarity of the hysteresis behavior at similar stresses suggests that, contrary to what was implied in a previous paper on this material, the large back-stress effect is not unique to partially recrystallized microstructures and is more broadly indicative of the large internal stresses that can be generated at dislocation obstacles in stronger materials. The evolutions of the back-stress and anelastic strain, as a function of both true strain and true stress, were measured for both conditions and are further discussed in the supplementary information (Fig. S4).

To further understand the accumulation of plastic deformation in the partially recrystallized microstructures, SEM-DIC was used to produce full-field strain maps in conjunction with EBSD observations. Testing was performed on the slow-ramp 600 °C/4 h condition because approximately 50% of the surface area was

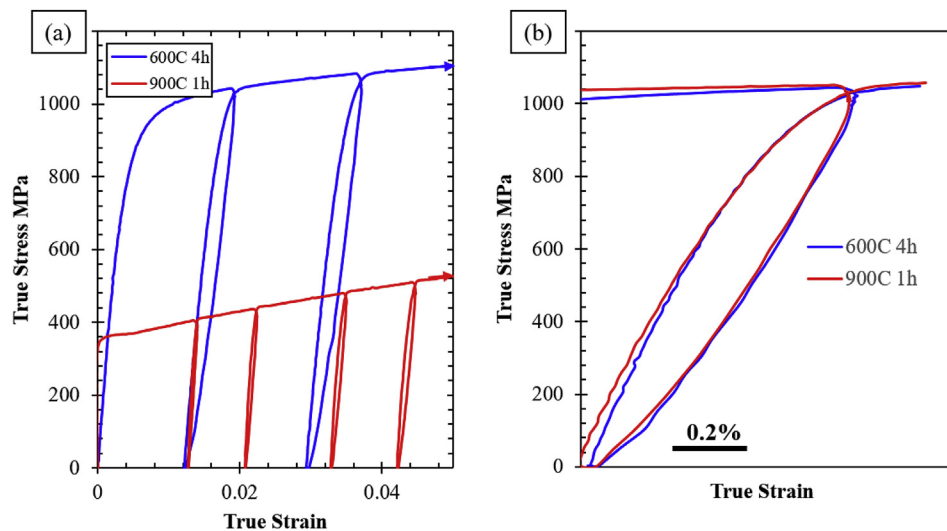


**Fig. 7.** Hysteresis behavior during load-unload-reload (LUR) tensile tests for partially recrystallized (blue) and fully recrystallized (red) conditions. The curves in (a) show that, at similar strains, the hysteresis behavior is much less pronounced in the fully recrystallized condition; the curves in (b) show that for similar stress levels, the hysteresis behavior is essentially identical for the two microstructural states. (For interpretation of the references to colour in this figure legend, the reader is referred to the Web version of this article.)

recrystallized, which produced sufficiently large regions of both recrystallized and non-recrystallized grains for facile measurement of the strain response. Fig. 8a shows a BSE-SEM image of a region containing both types of grains, where labels A and B denote recrystallized regions and labels C and D denote non-recrystallized regions. The white square at the top center of the image is a 2  $\mu\text{m}$  thick Pt deposit used for locating the same region on successive tests and assisting in image registration. Details of the test including the colloidal alumina pattern on the specimen surface used for DIC (Fig. 8b) and a representative stress-strain curve (Fig. 8c) are also shown. Fig. 8d shows a full-field strain map at an average macroscopic strain of 3.2%, as determined by macro-scale DIC over the entire region of uniform elongation in the gauge section. Since macroscopic yielding for this specimen occurred at 884 MPa/0.6% DIC elongation, as defined by the conventional 0.2% offset method, the expected plastic strain (total minus elastic) across the whole region of interest after unloading was 2.6%. This compared favorably to an average strain of 2.5% with standard deviation 1.0%, as measured via SEM-DIC. To estimate the error involved in the *ex situ* measurement method, images were also acquired for a reference sample with the same type of pattern and using the same beam conditions. The reference pattern was not deformed or otherwise altered between image acquisitions so the expected average strain was zero and any measured deformation was therefore taken as error. As previously noted, these errors are due to spatially-variable distortions introduced by the SEM. For the reference pattern recorded concurrently with the post-deformation pattern in Fig. 8d, the average erroneous strain parallel to the tensile axis was 0.08% with a standard deviation of 0.24%. Thus, the local strains displayed are well above this estimated error in the measurement.

As shown in Fig. 8d, substantial variations in plastic strain were observed across the region of interest. The overlaid grain boundary map shows that recrystallized regions deformed much more than non-recrystallized grains; for example, the local strains at recrystallized regions A and B were 4.7% and 4.5%, respectively. In contrast, the local strains in non-recrystallized regions C and D were 0.4% and 0.6%, an order of magnitude smaller. This indicates that non-recrystallized grains essentially behave as non-deformable inclusions at low strains; presumably, these retain a yield strength similar to the as-rolled material. Even within the recrystallized grains, the strain distribution was not uniform. Many grains showed strain values close to the macroscopic average; most regions where strain was higher than the macroscopic average (including regions A and B) were near or between non-recrystallized grains. The lack of deformation in the latter likely forces the adjacent recrystallized grains to undergo greater deformation to maintain compatibility.

#### 4. Discussion

There is a strong relationship between the tensile properties and fraction of recrystallized material in the equiatomic CrCoNi alloy. As noted earlier (Fig. 4), the grain size distribution of the fully recrystallized 700 °C/1 h condition is very similar to the recrystallized grains in the other heterogeneous conditions. Since the smaller grains do not exhibit substantial growth, it is also therefore expected that the size distribution of the non-recrystallized grains does not appreciably change from the as-rolled state during annealing. One important question is therefore whether the various partially recrystallized conditions behave as interpolations of the two bounding conditions (as-rolled and fully recrystallized), assuming similar grain size distributions. While some recovery is expected in the non-recrystallized grains, which would violate the assumption of fixed bounding conditions, it is clear (e.g. from Fig. 2)

that deformation structures like nanotwin/hcp lamellae remain and these structures are presumed to provide a majority of the strengthening contribution.

Fig. 9 shows the variation in yield strength (YS), ultimate tensile strength (UTS), uniform elongation (UE), and total elongation (TE) as a function of recrystallized fraction. These quantities vary monotonically but are not strictly linear, which may be in part the result of the anomalous hardening behavior observed at 600 °C. For example, it can be seen that the 600 °C/1 h condition (second point from the left, recrystallized fraction ~0.39) has higher strength and lower ductility than would be expected by a simple linear rule of mixtures model.

This can be further demonstrated by modeling the mechanical response of the partially recrystallized conditions as linear combinations of the as-rolled and fully recrystallized conditions. Note that this is only possible because of the similar grain size distributions for recrystallized grains (despite different recrystallized fractions). Rule-of-mixtures models were developed by interpolating the engineering stress-strain data for the two bounding conditions, weighting each according to the recrystallized fraction for a given condition, then summing the results at each interpolated point. For example, at 1% strain, the average interpolated stress for the fully recrystallized 700 °C/1 h condition was 694 MPa and the average interpolated stress for the as-rolled condition was 1284 MPa. Using the rule of mixtures model described above for the 600 °C/4 h condition, which had a recrystallized fraction of 76%, the expected stress corresponding to 1% strain would be  $(694 \text{ MPa} \cdot 0.76) + (1284 \text{ MPa} \cdot [1 - 0.76]) = 838 \text{ MPa}$ . This is somewhat lower than the observed value of 893 MPa (the average of three tests). The results for three different partially recrystallized conditions are shown in Fig. 10 where the solid curves indicate experimental data and the dashed curves are the predictions made by the rule-of-mixtures model. This simple model successfully captures the flow stress for the 650 °C/1 h but underestimates values for the 600 °C/1 h and 600 °C/4 h conditions. The results from Figs. 9 and 10 suggest that while the recrystallized fraction substantially affects the yield strength and other mechanical properties, other factors such as the anomalous hardening effect shown in Fig. 5 may also be important. Although the rule of mixtures model is not intended to be a rigorous predictive tool, it demonstrates that the response of the partially recrystallized material can be reasonably treated as a composite of the as-rolled material and fully recrystallized material.

This interpretation is also supported by the DIC strain map results. Although further testing at larger strains will be required to confirm the hypothesis, it presently appears that the behavior of recrystallized and non-recrystallized grains in a composite, heterogeneous structure is fundamentally similar to that in homogeneous alloys after accounting for the level of deformation. There does not appear to be a need to invoke long-range back-stresses or other exotic phenomena to explain the composite response. This does not suggest that long-range back-stresses are trivial; on the contrary, the results of the load-unload-reload tests indicate that very substantial back-stresses develop in CrCoNi even for initially homogeneous material. This may be a result of deformation twin/hcp lamellae that develop during testing and have previously been shown to act as profound barriers to dislocation motion [21,25]. Since these obstacles can potentially sustain extraordinarily large local shear stresses, they may also enable the development of very large back-stresses associated with dislocation tangles and pile-ups. Based on observations in the current work, these twin/hcp structures are known to be present after rolling and annealing but develop gradually during testing in the initially homogeneous microstructure. If the twin/hcp lamellae control the back-stress behavior, this may explain the initial difference in the hysteresis

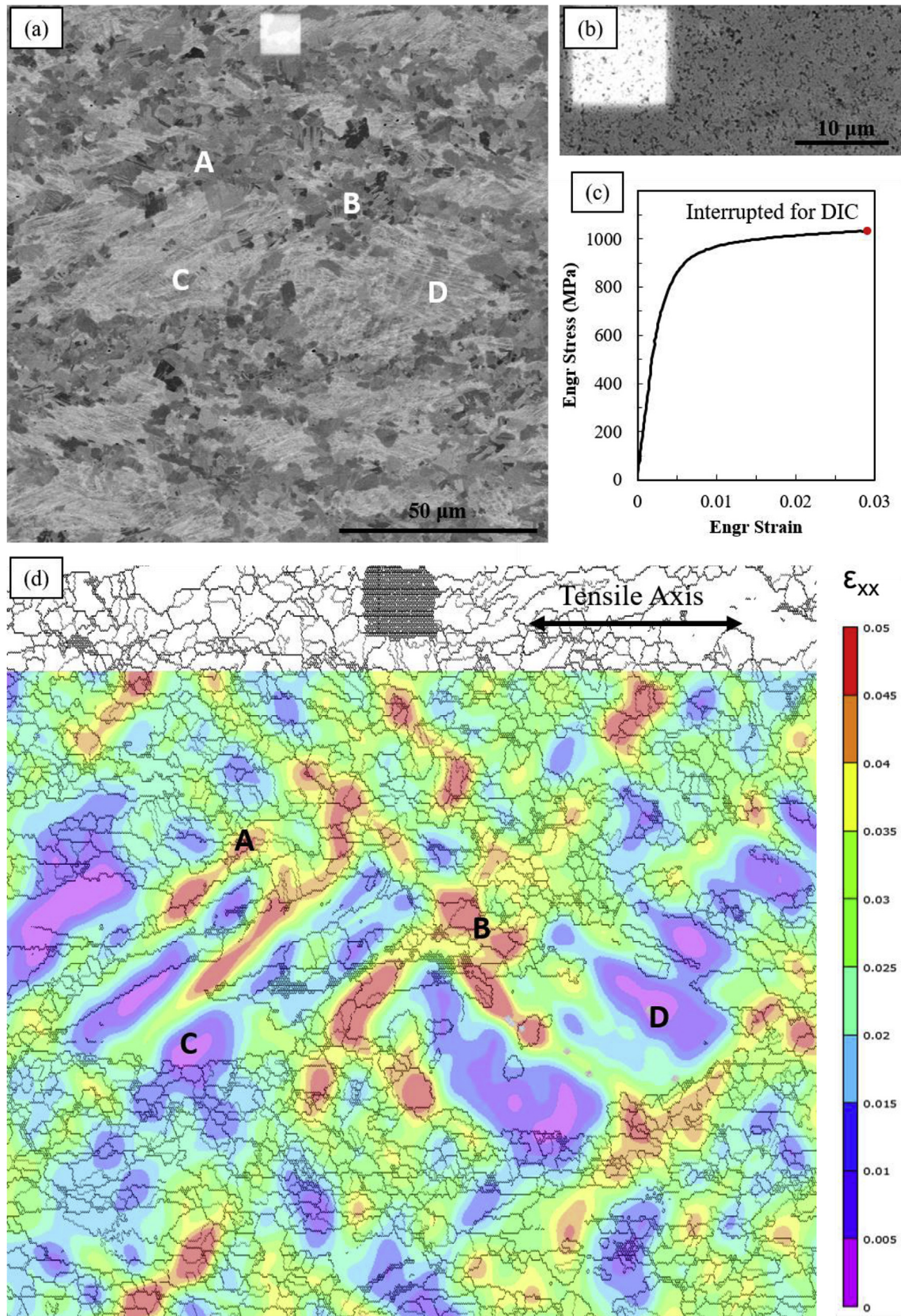


**Fig. 8.** Micro-DIC results for a rolled specimen annealed at 600C/4 h. (a) SEM-BSE micrograph showing the partially recrystallized microstructure with a Pt fiducial marker (white square at top). (b) The same region at higher magnification after patterning with colloidal alumina. (c) The engineering stress-strain curve for the interrupted test. (d) Micro-DIC strain map showing large differences in local strain between RX and non-RX regions.

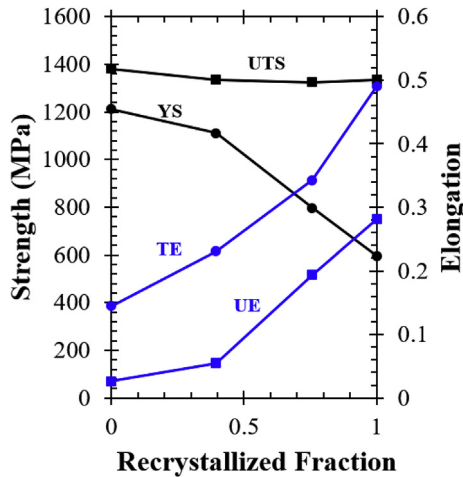


**Fig. 9.** Yield strength, ultimate tensile strength (true stress), uniform elongation (true strain), and total elongation (engineering strain) as a function of recrystallized fraction.

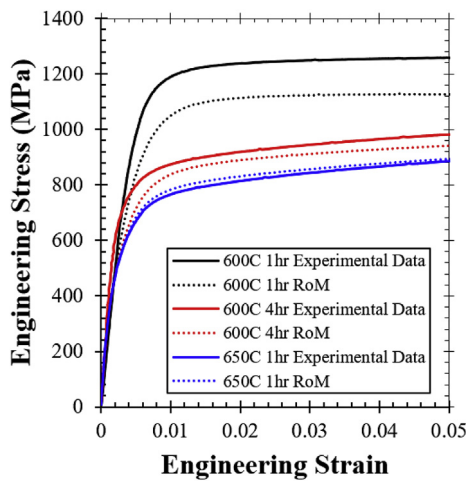


**Fig. 10.** Comparison of experimental data (solid curves) to predictions (dashed curves) based on rule-of-mixtures weighted average of the as-rolled material and the material annealed at 700C/1 h. Weighting was based on the amount of recrystallized grains: zero in the as-rolled material, 100% in the fully recrystallized material and various values in between for the other annealing conditions.

response followed by the similarity at higher stress.

Although there may be some benefit to having a structure with a bimodal or multi-modal grain size distribution, independent of the un-recovered deformation structure within some grains, that effect does not clearly appear here. In the present study, it appears that the outstanding mechanical properties can be explained in large part by the fraction of recrystallized material, and to some degree by the anomalous hardening response exhibited around 600 °C. It is, however, critical to distinguish this from the effect of grain refinement alone. Comparison of the mechanical properties from this work to the Hall-Petch study of equiatomic CrCoNi by Yoshida et al. [18] clearly demonstrates that these heterogeneous microstructures produce greater uniform elongation than homogeneous ultra-fine grain microstructures having similar yield strengths. For example, they reported a yield strength of approximately 1080 MPa for a homogeneous grain size of 199 nm; based on the provided plot, the estimated uniform elongation was less than 3% and the total elongation was less than 20%. In the current work, the 600 °C/1 h condition had an average yield strength of 1112 MPa with 6%

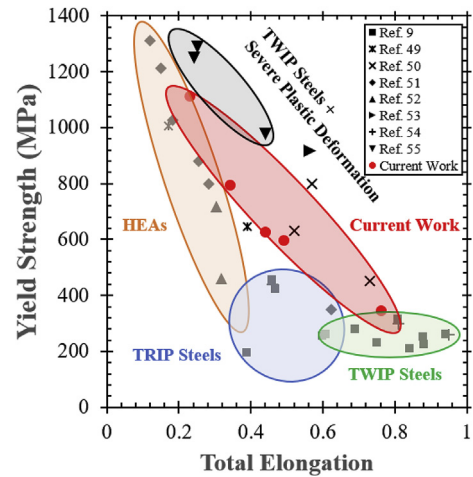


**Fig. 11.** Comparison of results from the current work (red) to other recent structural alloys. (For interpretation of the references to colour in this figure legend, the reader is referred to the Web version of this article.)

uniform elongation and 23% total elongation. The stress-strain curves are directly compared in Fig. S3c in the supplementary information.

The mechanical properties of the CrCoNi alloy, particularly with partially recrystallized microstructures, compare very favorably to other advanced structural materials. Fig. 11 shows a comparison of the yield strength and total elongation (for a variety of partially-recrystallized states) from the current work to several other high entropy alloys, TWIP steels, and TRIP steels [49–55]. Further details on the compositions and test geometries for the compared alloys can be found in Table S1 in the supplementary information. Based on the findings in this work, it is expected that other fcc medium/high entropy alloys with similar deformation mechanisms could also be capable of dramatic increases in strength through the same rolling and annealing processing described here. This may be especially potent in the CrCoFeNi system since it also exhibits a nanoscale fcc-to-hcp transformation at large strains, and this strengthening phase remains in the non-recrystallized grains after annealing.

## 5. Conclusions

Despite having otherwise excellent mechanical properties, single-phase medium/high entropy alloys are limited by modest yield strengths. This work examined a simple processing route consisting of rolling and annealing of an equiatomic CrCoNi alloy to produce heterogeneous microstructures with very high yield strengths and large uniform elongations. The key results of this work were as follows:

- 1) Rolling and annealing produced partially recrystallized microstructures where non-recrystallized grains retained deformation twins and very high dislocation densities.
- 2) Hardness measurements and tensile testing of the partially recrystallized heterogeneous microstructures showed substantial improvements in the strength of the alloy with only modest compromises to ductility. The uniform elongation is better than in homogeneous microstructures with high yield strengths achieved through grain refinement alone.
- 3) Load-unload-reload testing showed that although substantial back-stresses, evidenced by large hysteresis loops, are present in the partially recrystallized material, the hysteresis behavior is

essentially identical to that in more conventional, fully recrystallized material when the two microstructural states are compared at similar stress levels. This suggests that high back-stress is not a unique feature of the heterogeneous microstructures.

- 4) Digital image correlation showed that recrystallized grains (which initially have very low dislocation densities) deform much more than non-recrystallized grains, which essentially act as hard inclusions. The macroscopic mechanical response of the heterogeneous microstructures can be reasonably treated as a rule-of-mixtures composite of the as-rolled and fully recrystallized material with a similar grain size.

## Acknowledgments

The National Science Foundation, Division of Materials Research is acknowledged for supporting CES and MJM (mechanical testing and SEM-level characterization) under contract #DMR-1508505. Funding for JM and TEM-level characterization supported under the GOALI DMREF program #DMR-1534826. CES was also supported by the National Science Foundation Graduate Research Fellowship Program Grant No. DGE-1343012. Any opinions, findings, and conclusions or recommendations expressed in this material are those of the authors and do not necessarily reflect the views of the National Science Foundation. Hamish Fraser and the Center for the Accelerated Maturation of Materials are thanked for access to mechanical testing facilities. EPG is sponsored by the U.S. Department of Energy, Office of Science, Basic Energy Sciences, Materials Sciences and Engineering Division.

## Appendix A. Supplementary data

Supplementary data to this article can be found online at <https://doi.org/10.1016/j.actamat.2018.12.015>.

## References

- [1] B. Gludovatz, A. Hohenwarter, K.V.S. Thurston, H. Bei, Z. Wu, E.P. George, R.O. Ritchie, Exceptional damage-tolerance of a medium-entropy alloy CrCoNi at cryogenic temperatures, *Nat. Commun.* 7 (2016) 10602, <https://doi.org/10.1038/ncomms10602>.
- [2] G. Laplanche, A. Kostka, C. Reinhart, J. Hunfeld, G. Eggeler, E.P. George, Reasons for the superior mechanical properties of medium-entropy CrCoNi compared to high-entropy CrMnFeCoNi, *Acta Mater.* 128 (2017) 292–303, <https://doi.org/10.1016/j.actamat.2017.02.036>.
- [3] J. Miao, C.E. Slone, T.M. Smith, C. Niu, H. Bei, M. Ghazisaeidi, G.M. Pharr, M.J. Mills, The evolution of the deformation substructure in a Ni-Co-Cr equiatomic solid solution alloy, *Acta Mater.* 132 (2017) 35–48, <https://doi.org/10.1016/j.actamat.2017.04.033>.
- [4] A. Gali, E.P. George, Tensile properties of high- and medium-entropy alloys, *Intermetallics* 39 (2013) 74–78, <https://doi.org/10.1016/j.intermet.2013.03.018>.
- [5] B. Gludovatz, A. Hohenwarter, D. Catoor, E.H. Chang, E.P. George, R.O. Ritchie, A fracture-resistant high-entropy alloy for cryogenic applications, *Science* (80- ) 345 (2014) 1153–1158, <https://doi.org/10.1126/science.1254581>.
- [6] G. Laplanche, A. Kostka, O.M. Horst, G. Eggeler, E.P. George, Microstructure evolution and critical stress for twinning in the CrMnFeCoNi high-entropy alloy, *Acta Mater.* 118 (2016) 152–163, <https://doi.org/10.1016/j.actamat.2016.07.038>.
- [7] B. Cantor, I.T.H. Chang, P. Knight, A.J.B. Vincent, Microstructural development in equiatomic multicomponent alloys, *Mater. Sci. Eng.* 375–377 (2004) 213–218, <https://doi.org/10.1016/j.msea.2003.10.257>.
- [8] Z. Wu, H. Bei, F. Otto, G.M. Pharr, E.P. George, Recovery, recrystallization, grain growth and phase stability of a family of FCC-structured multi-component equiatomic solid solution alloys, *Intermetallics* 46 (2014) 131–140, <https://doi.org/10.1016/j.intermet.2013.10.024>.
- [9] O. Grässel, L. Krüger, G. Frommeyer, L.W. Meyer, High strength Fe-Mn-(Al, Si) TRIP/TWIP steels development - properties - application, *Int. J. Plast.* 16 (2000) 1391–1409, [https://doi.org/10.1016/S0749-6419\(00\)00015-2](https://doi.org/10.1016/S0749-6419(00)00015-2).
- [10] I. Gutierrez-Urrutia, D. Raabe, Dislocation and twin substructure evolution during strain hardening of an Fe-22 wt.% Mn-0.6 wt.% C TWIP steel observed by electron channeling contrast imaging, *Acta Mater.* 59 (2011) 6449–6462, <https://doi.org/10.1016/j.actamat.2011.07.009>.
- [11] N.L. Okamoto, S. Fujimoto, Y. Kambara, M. Kawamura, Z.M.T. Chen, H. Matsunoshita, K. Tanaka, H. Inui, E.P. George, Size effect, critical resolved shear stress, stacking fault energy, and solid solution strengthening in the CrMnFeCoNi high-entropy alloy, *Sci. Rep.* 6 (2016) 1–10, <https://doi.org/10.1038/srep35863>.
- [12] S.H. Joo, H. Kato, M.J. Jang, J. Moon, C.W. Tsai, J.W. Yeh, H.S. Kim, Tensile deformation behavior and deformation twinning of an equimolar CoCr-FeMnNi high-entropy alloy, *Mater. Sci. Eng.* 689 (2017) 122–133, <https://doi.org/10.1016/j.msea.2017.02.043>.
- [13] W. Abuzaid, H. Sehitoglu, Critical resolved shear stress for slip and twin nucleation in single crystalline FeNiCoCrMn high entropy alloy, *Mater. Char.* 129 (2017) 288–299, <https://doi.org/10.1016/j.matchar.2017.05.014>.
- [14] W. Skrotzki, A. Pukenas, B. Joni, E. Odor, T. Ungar, A. Hohenwarter, R. Pippan, E.P. George, Microstructure and texture evolution during severe plastic deformation of CrMnFeCoNi high-entropy alloy, *IOP Conf. Ser. Mater. Sci. Eng.* 194 (2017), <https://doi.org/10.1088/1757-899X/194/1/012028>.
- [15] Z. Wu, H. Bei, G.M. Pharr, E.P. George, Temperature dependence of the mechanical properties of equiatomic solid solution alloys with face-centered cubic crystal structures, *Acta Mater.* 81 (2014) 428–441, <https://doi.org/10.1016/j.actamat.2014.08.026>.
- [16] Q. Lin, J. Liu, X. An, H. Wang, Y. Zhang, X. Liao, Cryogenic-deformation-induced phase transformation in an FeCoCrNi high-entropy alloy, *Mater. Res. Lett.* 6 (2018) 236–243, <https://doi.org/10.1080/21663831.2018.1434250>.
- [17] Z. Zhang, H. Sheng, Z. Wang, B. Gludovatz, Z. Zhang, E.P. George, Q. Yu, S.X. Mao, R.O. Ritchie, Dislocation mechanisms and 3D twin architectures generate exceptional strength-ductility-toughness combination in CrCoNi medium-entropy alloy, *Nat. Commun.* 8 (2017) 14390, <https://doi.org/10.1038/ncomms14390>.
- [18] S. Yoshida, T. Bhattacharjee, Y. Bai, N. Tsuji, Friction stress and Hall-Petch relationship in CoCrNi equi-atomic medium entropy alloy processed by severe plastic deformation and subsequent annealing, *Scripta Mater.* 134 (2017) 33–36, <https://doi.org/10.1016/j.scriptamat.2017.02.042>.
- [19] H. Huang, X. Li, Z. Dong, W. Li, S. Huang, D. Meng, X. Lai, T. Liu, S. Zhu, L. Vitos, Critical stress for twinning nucleation in CrCoNi-based medium and high entropy alloys, *Acta Mater.* 149 (2018) 388–396, <https://doi.org/10.1016/j.actamat.2018.02.037>.
- [20] S. Zhao, G.M. Stocks, Y. Zhang, Stacking fault energies of face-centered cubic concentrated solid solution alloys, *Acta Mater.* 134 (2017) 334–345, <https://doi.org/10.1016/j.actamat.2017.05.001>.
- [21] C. Niu, C.R. Larosa, J. Miao, M.J. Mills, M. Ghazisaeidi, Magnetically-driven phase transformation strengthening in high entropy alloys, *Nat. Commun.* 9 (2018).
- [22] S.F. Liu, Y. Wu, H.T. Wang, J.Y. He, J.B. Liu, C.X. Chen, X.J. Liu, H. Wang, Z.P. Lu, Stacking fault energy of face-centered-cubic high entropy alloys, *Intermetallics* 93 (2018) 269–273, <https://doi.org/10.1016/j.intermet.2017.10.004>.
- [23] C.L. Tracy, S. Park, D.R. Rittman, S.J. Zinkle, H. Bei, M. Lang, R.C. Ewing, W.L. Mao, High pressure synthesis of a hexagonal close-packed phase of the high-entropy alloy CrMnFeCoNi, *Nat. Commun.* 8 (2017) 1–6, <https://doi.org/10.1038/ncomms15634>.
- [24] F. Zhang, Y. Wu, H. Lou, Z. Zeng, V.B. Prakapenka, E. Greenberg, Y. Ren, J. Yan, J.S. Okasinski, X. Liu, Y. Liu, Q. Zeng, Z. Lu, Polymorphism in a high-entropy alloy, *Nat. Commun.* 8 (2017) 1–7, <https://doi.org/10.1038/ncomms15687>.
- [25] C.E. Slone, S. Chakraborty, J. Miao, E.P. George, M.J. Mills, S.R. Niezgodna, Influence of deformation induced nanoscale twinning and FCC-HCP transformation on hardening and texture development in medium-entropy CrCoNi alloy, *Acta Mater.* 158 (2018) 38–52, <https://doi.org/10.1016/j.actamat.2018.07.028>.
- [26] O. Bouaziz, C.P. Scott, G. Petitgand, Nanostructured steel with high work-hardening by the exploitation of the thermal stability of mechanically induced twins, *Scripta Mater.* 60 (2009) 714–716, <https://doi.org/10.1016/j.scriptamat.2009.01.004>.
- [27] C. Haase, T. Ingendahl, O. Güvenç, M. Bambach, W. Bleck, D.A. Molodov, L.A. Barrales-Mora, On the applicability of recovery-annealed Twinning-Induced Plasticity steels: potential and limitations, *Mater. Sci. Eng.* 649 (2016) 74–84, <https://doi.org/10.1016/j.msea.2015.09.096>.
- [28] F. Berrenberg, C. Haase, L.A. Barrales-Mora, D.A. Molodov, Enhancement of the strength-ductility combination of twinning-induced/transformation-induced plasticity steels by reversion annealing, *Mater. Sci. Eng.* 681 (2017) 56–64, <https://doi.org/10.1016/j.msea.2016.10.109>.
- [29] A. Mandal, S. Patra, D. Chakraborty, S.B. Singh, Effect of rolling and subsequent annealing on microstructure, microtexture, and properties of an experimental duplex stainless steel, *Metall. Mater. Trans. A Phys. Metall. Mater. Sci.* 48 (2017) 5960–5977, <https://doi.org/10.1007/s11661-017-4345-x>.
- [30] F. Brasche, C. Haase, L.A. Barrales-Mora, D.A. Molodov, Comparative study of the influence of reversion- and recovery- annealing on the mechanical behavior of high-manganese steels with varying stacking fault energy, *Steel Res. Int.* (2017), <https://doi.org/10.1002/srin.201700377>.
- [31] Y.H. Jo, S. Jung, W.M. Choi, S.S. Sohn, H.S. Kim, B.J. Lee, N.J. Kim, S. Lee, Cryogenic strength improvement by utilizing room-temperature deformation twinning in a partially recrystallized CrMnFeCoNi high-entropy alloy, *Nat. Commun.* 8 (2017) 1–8, <https://doi.org/10.1038/ncomms15719>.
- [32] C. Haase, L.A. Barrales-mora, Influence of deformation and annealing twinning on the microstructure and texture evolution of face-centered cubic high-entropy alloys, *Acta Mater.* 150 (2018) 1–42, <https://doi.org/10.1016/j.actamat.2018.02.037>.

- [j.actamat.2018.02.048](https://doi.org/10.1016/j.actamat.2018.02.048).
- [33] C.E. Slone, J. Miao, M.J. Mills, Ultra-high strength and ductility from rolling and annealing of a Ni-Cr-Co superalloy, *Scripta Mater.* 155 (2018) 94–98, <https://doi.org/10.1016/j.scriptamat.2018.06.033>.
- [34] B. Schuh, B. Volker, J. Todt, K.S. Kormout, N. Schell, A. Hohenwarter, Influence of annealing on microstructure and mechanical properties of a nanocrystalline CrCoNi medium-entropy alloy, *Materials* 11 (2018), <https://doi.org/10.1007/s11661-018-4472-z>.
- [35] Y. Ma, F. Yuan, M. Yang, P. Jiang, E. Ma, X. Wu, Dynamic shear deformation of a CrCoNi medium-entropy alloy with heterogeneous grain structures, *Acta Mater.* 148 (2018) 407–418, <https://doi.org/10.1016/j.actamat.2018.02.016>.
- [36] M. Yang, D. Yan, F. Yuan, P. Jiang, E. Ma, X. Wu, Dynamically reinforced heterogeneous grain structure prolongs ductility in a medium-entropy alloy with gigapascal yield strength, *Proc. Natl. Acad. Sci. Unit. States Am.* (2018), 201807817, <https://doi.org/10.1073/pnas.1807817115>.
- [37] Vic-2D 2009. Version 2009.1.0, Build 933., Correlated Solutions, Inc. Irmo, South Carolina.
- [38] OIM Analysis, Version 8.0, 2016., AMETEK, Inc. EDAX, Inc., Mahwah, NJ.
- [39] C. Ophus, J. Ciston, C.T. Nelson, Correcting nonlinear drift distortion of scanning probe and scanning transmission electron microscopies from image pairs with orthogonal scan directions, *Ultramicroscopy* 162 (2016) 1–9, <https://doi.org/10.1016/j.ultramicro.2015.12.002>.
- [40] J. Miao, C.E. Slone, T.M. Smith, C. Niu, H. Bei, M. Ghazisaeidi, G.M. Pharr, M.J. Mills, The evolution of the deformation substructure in a Ni-Co-Cr equiatomic solid solution alloy, *Acta Mater.* 132 (2017), <https://doi.org/10.1016/j.actamat.2017.04.033>.
- [41] F. Yin, A. Sakurai, X. Song, Determination of spatial grain size with the area-weighted grain area distribution of the planar sections in polycrystalline materials, *Metall. Mater. Trans. A Phys. Metall. Mater. Sci.* 37 (2006) 3707–3714, <https://doi.org/10.1007/s11661-006-1064-0>.
- [42] A. Berger, M. Herwegh, J.O. Schwarz, B. Putlitz, Quantitative analysis of crystal/grain sizes and their distributions in 2D and 3D, *J. Struct. Geol.* 33 (2011) 1751–1763, <https://doi.org/10.1016/j.jsg.2011.07.002>.
- [43] L.S. Toth, S. Biswas, C. Gu, B. Beausir, Notes on representing grain size distributions obtained by electron backscatter diffraction, *Mater. Char.* 84 (2013) 67–71, <https://doi.org/10.1016/j.matchar.2013.07.013>.
- [44] F. Otto, N.L. Hanold, E.P. George, Microstructural evolution after thermo-mechanical processing in an equiatomic, single-phase CoCrFeMnNi high-entropy alloy with special focus on twin boundaries, *Intermetallics* 54 (2014) 39–48, <https://doi.org/10.1016/j.intermet.2014.05.014>.
- [45] B. Schuh, F. Mendez-Martin, B. Völker, E.P. George, H. Clemens, R. Pippan, A. Hohenwarter, Mechanical properties, microstructure and thermal stability of a nanocrystalline CoCrFeMnNi high-entropy alloy after severe plastic deformation, *Acta Mater.* 96 (2015) 258–268, <https://doi.org/10.1016/j.actamat.2015.06.025>.
- [46] C. Haase, L.A. Barrales-Mora, Influence of deformation and annealing twinning on the microstructure and texture evolution of face-centered cubic high-entropy alloys, *Acta Mater.* 150 (2018) 88–103, <https://doi.org/10.1016/j.actamat.2018.02.048>.
- [47] G.E. Dieter, *Mechanical Metallurgy*, third ed., 1988.
- [48] D. Barbier, N. Gey, S. Allain, N. Bozzolo, M. Humbert, Analysis of the Tensile Behavior of a TWIP Steel Based on the Texture and Microstructure Evolutions, vol. 500, 2009, pp. 196–206, <https://doi.org/10.1016/j.msea.2008.09.031>.
- [49] J.Y. He, H. Wang, H.L. Huang, X.D. Xu, M.W. Chen, Y. Wu, X.J. Liu, T.G. Nieh, K. An, Z.P. Lu, A precipitation-hardened high-entropy alloy with outstanding tensile properties, *Acta Mater.* 102 (2016) 187–196, <https://doi.org/10.1016/j.actamat.2015.08.076>.
- [50] J.B. Seol, J.W. Bae, Z. Li, J. Chan Han, J.G. Kim, D. Raabe, H.S. Kim, Boron doped ultrastrong and ductile high-entropy alloys, *Acta Mater.* 151 (2018) 366–376, <https://doi.org/10.1016/j.actamat.2018.04.004>.
- [51] K. Ming, X. Bi, J. Wang, Precipitation strengthening of ductile Cr15Fe20-Co35Ni20Mo10 alloys, *Scripta Mater.* 137 (2017) 88–93, <https://doi.org/10.1016/j.scriptamat.2017.05.019>.
- [52] Z.G. Wang, W. Zhou, L.M. Fu, J.F. Wang, R.C. Luo, X.C. Han, B. Chen, X.D. Wang, Effect of coherent L1<sub>2</sub> nanoprecipitates on the tensile behavior of a fcc-based high-entropy alloy, *Mater. Sci. Eng.* 696 (2017) 503–510, <https://doi.org/10.1016/j.msea.2017.04.111>.
- [53] X. Li, R. Song, N. Zhou, J. Li, An ultrahigh strength and enhanced ductility cold-rolled medium-Mn steel treated by intercritical annealing, *Scripta Mater.* 154 (2018) 30–33, <https://doi.org/10.1016/j.scriptamat.2018.05.016>.
- [54] G. Frommeyer, U. Brüx, P. Neumann, Supra-Ductile and high-strength manganese-TRIP/TWIP steels for high energy, *Absorp. Purpos.* 43 (2003) 438–446.
- [55] I.B. Timokhina, A. Medvedev, R. Lapovok, Severe plastic deformation of a TWIP steel, *Mater. Sci. Eng.* 593 (2014) 163–169, <https://doi.org/10.1016/j.msea.2013.11.013>.